

Data Repository Items

METHODS

Approximately 3–10 kg of sample were crushed using a jaw crusher and disc grinder and processed for mineral separations using a Gemini water table. Zircons were concentrated using sodium polytungstate, methylene iodide, and magnetic separation with a Frantz.

LA-MC-ICPMS

For LA-MC-ICPMS analysis, all material that sank in MEI and was non-magnetic at 1.0 A was put on 2.5 cm epoxy mounts. Beam diameter was 35 mm. The ablated material was transported in an Ar-He carrier gas into the plasma source of a GV Instruments Isoprobe, which is equipped with a flight tube of sufficient width to allow simultaneous analysis of U, Th, and Pb isotopes. All measurements were made in static mode, using Faraday detectors for ^{238}U , ^{232}Th , $^{208\text{-}206}\text{Pb}$, and an ion-counting channel for ^{204}Pb . Ion yields were ~1 mv per ppm. Each analysis consisted of an integrated 20-second background measurement on the peak positions, 20 one-second integrations with the laser firing, and a 30 second delay to purge the previous sample and prepare for the next analysis.

Common Pb corrections were made using measured ^{204}Pb concentrations and assuming an initial Pb composition from Stacey and Kramers (1975) with uncertainties of 1.0 for $^{206}\text{Pb}/^{204}\text{Pb}$ and 0.3 for $^{207}\text{Pb}/^{204}\text{Pb}$. The Ar-He carrier gas contains negligible ^{204}Hg and we corrected for isobaric ^{204}Hg interferences on ^{204}Pb as part of the background measurements.

Elemental fractionation for LA-MC-ICPMS varies with pit depth and the accepted isotope ratios were determined by least-squares projection through the measured values back to the initial determination. Inter-element fractionation of Pb/U was generally <20%, whereas apparent fractionation of Pb isotopes was generally <5%. Each analysis was normalized to the University of Arizona "SL" zircon standard with an age of 564 ± 4 Ma (Gehrels et al., 2008), which was analyzed after every fifth sample analysis for detrital zircons and every fourth analysis for igneous zircons. Zircon standard "R33" was also analyzed during these sessions. The uncertainty resulting from the calibration correction (together with the uncertainty from decay constants and common Pb composition) is generally 1-2% (2s) for $^{206}\text{Pb}/^{238}\text{U}$ and $^{207}\text{Pb}/^{206}\text{Pb}$ ages of >1.2 Ga.

Errors from the measurement of $^{206}\text{Pb}/^{238}\text{U}$, $^{206}\text{Pb}/^{207}\text{Pb}$, and $^{206}\text{Pb}/^{204}\text{Pb}$ are reported at the 1s level. Additional errors that affect all ages include uncertainties from (1) U decay constants; (2) the composition of common Pb; (3) calibration correction; and (4) uncertainty in age of the standard. These systematic errors (SE) are not included in the tables and add an additional uncertainty to $^{206}\text{Pb}/^{238}\text{U}$ ages and $^{207}\text{Pb}/^{206}\text{Pb}$ ages. Interpreted ages for igneous rocks incorporate the systematic errors into the weighted mean ages so that the total 2s uncertainties that are quoted are equal to the quadratic sum of the random plus systematic errors. U and Th concentrations have approximately 25% uncertainty. Analyses with >10% 1s uncertainty, >30% normal discordance, or >5% reverse discordance are excluded from the plots and interpretations. Relative probability diagrams and weighted mean calculations were created using the Isoplot program

(Ludwig, 2003). Other details of analytical methods are given elsewhere (Gehrels et al., 2006; Gehrels et al., 2008; Gehrels et al., 2011).

The total number of analyses from each sample was highly variable. It is desirable and recommended that 100 analyses be obtained from each sample for detrital zircon age analysis, but financial limitations prevented us from reaching this total on every sample.

SHRIMP

U-Pb dating of igneous rocks was conducted using the USGS/Stanford sensitive high-resolution ion microprobe-reverse geometry (SHRIMP-RG) at Stanford University. The primary beam excavated an area of about 25–30 μm across to a depth of about 1 μm . Zircons were hand-picked, mounted in epoxy, ground to half-thickness, and polished with 6 μm and 1 μm diamond suspension. All grains were imaged in reflected and transmitted light on a petrographic microscope and in cathodoluminescence (CL) on a scanning electron microscope. The analytical routine followed Williams (1998) and Barth et al. (2001). Data reduction utilized the SQUID program of Ludwig (2005). The concentration of U was calibrated using zircon standard CZ3 ($\text{U} = 550 \text{ ppm}$). Isotopic compositions were calibrated by replicate analyses of zircon standard R33 that has an age of 419 Ma (Black et al., 2004). Calibration error for the $^{206}\text{Pb}/^{238}\text{U}$ ratios of R33 for the analytical session was 0.38% (2s). Discussion and interpretation of analyses are based on $^{206}\text{Pb}/^{238}\text{U}$ ages calculated from ratios corrected for common Pb using the ^{207}Pb method. Common Pb compositions were estimated from Stacey and Kramers (Stacey and Kramers, 1975).

For SHRIMP analysis, zircons were hand picked from material that sank in MEI and was non-magnetic at 1.8 A. About 30–50 zircons were put on 2.5 cm epoxy mounts for individual analysis. Samples were analyzed in two separate sessions in 2007 and 2009. A 30-mm diameter, 8–12 nA O₂ primary beam was used to sputter the zircon grains for analysis, following 90 seconds of rastering to remove potential surface contamination. CL images were obtained for all zircons analyzed. U, Th, and Pb concentrations were standardized against RG-6 and VP-10 zircons that were analyzed after every four unknown analyses. Data was reduced using the SQUID program (Ludwig, 2001). Pb/U ratios were corrected for common Pb using the model Pb evolution curve of Stacey and Kramers (1975). Errors on spot ages of individual zircon grains are reported at 1s, and weighted mean ages were calculated and reported in the text and figures at the 2s level. The weighted mean of $^{207}\text{Pb}/^{206}\text{Pb}$ ages derived using the SQUID and Isoplot programs incorporates uncertainties in the standards and decay constants into the reported errors and thus the total uncertainties reported are comparable in scope to those reported from the LA-ICPMS data.

Zircon data in Table DR1 is presented in the same order as in Table 1.

DETAILED DESCRIPTIONS OF THE STUDY AREAS

San Andres Mountains

Proterozoic rocks of the San Andres Mountains are exposed at the base of the eastern flank of west-tilted fault blocks below an unconformity with the Bliss Sandstone (Kottlowski et al., 1956; Bachman and Harbour, 1970; Condie and Budding, 1979;

Seager, 1981; Vollbrecht, 1997). Metamorphosed igneous and metasedimentary rocks include gneiss, granite, amphibolite, and metavolcanic rocks. Foliated granites have been dated at 1675–1620 Ma (Roths, 1991; Vollbrecht, 1997; Amato et al., 2008) with younger undeformed granitic plutons as the 1462 Ma (Roths, 1991). Quartzite from the area had a single population of detrital zircons at 1670 Ma (Amato et al., 2008). The Bliss Sandstone overlies Proterozoic granite and schist and ranges in thickness from 35 m in the south to 2–5 m in the northern San Andres Mts. and pinches out in the Oscura Mts. 100 km to the north (Bachman and Myers, 1969; Bachman and Harbour, 1970). Bachman and Myers (1969) describe a lower section of ledge-forming yellow-gray fine-grained quartzite overlain by sandstone-quartzite-shaly sandstone with quartz-pebble conglomerate near the base of the upper section. The Bliss is overlain with a gradational contact by the El Paso formation. Sample 10SA-10 overlies foliated granite dated at 1632 Ma (Roths, 1991). Sample 04SASC-6 overlies granitic rocks of unknown age (Bachman and Myers, 1969).

San Diego Mountain

San Diego Mountain, also known as Tonuco Mountain, consists of Proterozoic granite overlain by Bliss Sandstone that grades into Ordovician El Paso Limestone (Seager et al., 1971). The Bliss Sandstone is approximately 40 m thick and is consists of hematitic quartz sandstone with glauconite; fossils include brachiopods and trilobites indicating a Late Cambrian age for the lower beds and Early Ordovician age for the upper beds (Seager et al., 1971). The underlying granite was dated as part of this study (see below).

Mud Springs

The Mud Springs Mountains exposes a tilted fault block of Precambrian basement overlain by Bliss Sandstone and Paleozoic rocks of Ordovician, Devonian, Pennsylvanian, and Permian age (Maxwell and Oakman, 1990). The Precambrian rocks are mapped as quartzite, schist, amphibolite, and granite gneiss (Maxwell and Oakman, 1990), which are likely ~1.65 Ga in age based on the ages of similar rocks in the Burro Mountains (Amato et al., 2008).

San Lorenzo

The Bliss Sandstone at this locality was collected approximately 2 km southwest of the town of San Lorenzo, New Mexico, and overlies Precambrian rocks mapped as amphibolite (Hedlund, 1977). These rocks are undated but also likely ~1.65 Ga in age.

Florida Mountains

A small outcrop of Paleoproterozoic granite orthogneiss is cut by amphibolite dikes (Clemons, 1998). The orthogneiss that originally yielded an age of 1570–1550 Ma from discordant zircons (Evans and Clemons, 1988). Another sample from this exposure was redated and yielded ages of about 1.67–1.65 Ga (Amato et al., 2008; but see below). Cambrian granite, originally dated by Evans and Clemons (1988), was redated as part of this study (see below). It is overlain by Bliss Sandstone that grades into El Paso limestone. The Bliss ranges in thickness from 0–60 m, variations related to relief on the

unconformity (Evans and Clemons, 1988). Boulders of the Florida granite are present in some of the basal Bliss units (Clemons, 1998).

Burro Mountains

Proterozoic metamorphic rocks >1.6 Ga were intruded by abundant ~1.4 Ga plutons (Amato et al., 2008; Amato et al., 2011). The Bliss Sandstone exposures are limited to a small outcrop on the southwest side of the range and several larger outcrops, the largest of which is approximately 500 m across, on the eastern side (Fig. 2). Bedding on the west side dips 40° west (Hedlund, 1978a) and bedding on the east side dips ~15°east (Hedlund, 1978b; this study). Ordovician El Paso limestone conformably overlies the Bliss Sandstone. Granite underneath the unconformity was dated as part of this study (see below).

Little Hatchet Mountains

Bliss Sandstone overlies Proterozoic igneous rocks including a rapakivi granite, dated as part of this study, that was intruded by aplite dikes at 1080 Ma (Clinkscales and Lawton, 2011). The Bliss is about 60 m in thickness, and we sampled about 15 m above the base.

REFERENCES CITED

- Amato, J. M., Boullion, A. O., Serna, A. M., Sanders, A. E., Farmer, G. L., Gehrels, G. E., and Wooden, J. L., 2008, The evolution of the Mazatzal province and the timing of the Mazatzal orogeny: Insights from U-Pb geochronology and geochemistry of igneous and metasedimentary rocks in southern New Mexico: Geological Society of America Bulletin, v. 120, p. 328-346.
- Amato, J. M., Heizler, M. T., Boullion, A. O., Sanders, A. E., Toro, J., McLemore, V. T., and Andronicos, C. L., 2011, Syntectonic 1.46 Ga magmatism and rapid cooling of a gneiss dome in the southern Mazatzal Province: Burro Mountains, New Mexico: Geological Society of America Bulletin, v. 123, p. 1720-1744.
- Bachman, G. O., and Harbour, R. L., 1970, Geologic map of the northern part of the San Andres Mountains, central New Mexico: U. S. Geological Survey Miscellaneous Geologic Investigations, Map I-600, scale 1:62,500.
- Bachman, G. O., and Myers, D. A., 1969, Geology of the Bear Peak Area, Dona Ana County New Mexico: U. S. Geological Survey Bulletin 1271-C, p. 46 pp.
- Barth, A. P., Wooden, J. L., and Coleman, D. S., 2001, SHRIMP-RG U-Pb zircon geochronology of Mesoproterozoic metamorphism and plutonism in the southwesternmost United States: Journal of Geology, v. 109, p. 319-327.
- Black, L. P., Kamo, S. L., Allen, C. M., Davis, D. W., Aleinikoff, J. N., Valley, J. W., Mundil, R., Campbell, I. H., Korsch, R. J., Williams, I. S., and Foudoulis, C., 2004, Improved 206Pb/238U microprobe geochronology by the monitoring of a trace-element related matrix effect; SHRIMP, ID-TIMS, ELA-ICP-MS and oxygen isotope documentation for a series of zircon standards: Chemical Geology, v. 205, p. 115–140.
- Clemons, R. E., 1998, Geology of the Florida Mountains, southwestern New Mexico: New Mexico Bureau of Mines and Mineral Resources Memoir, v. 43, p. 112.

- Clinkscales, C. A., and Lawton, T. F., 2011, New constraints on the kinematic and paleogeographic history of the Little Hatchet Mountains, southwestern New Mexico: *New Mexico Geology*, v. 33, no. 2, p. 49.
- Condie, K. C., and Budding, A. J., 1979, Geology and geochemistry of Precambrian rocks, central and south-central New Mexico: *New Mexico Bureau of Mines and Mineral Resources Memoir*, v. 25, p. 1-58.
- Evans, K. V., and Clemons, R. E., 1988, Cambrian-Ordovician (500 Ma) alkalic plutonism in southwestern New Mexico: U-Th-Pb isotopic data from the Florida Mountains: *American Journal of Science*, v. 288, p. 735-755.
- Gehrels, G. E., Valencia, V., and Ruiz, J., 2008, Enhanced precision, accuracy, efficiency, and spatial resolution of U-Pb ages by laser ablation–multicollector–inductively coupled plasma–mass spectrometry: *Geochemistry, Geophysics, Geosystems (G-cubed)*, v. 9.
- Hedlund, D. C., 1977, Geology of the Hillsboro and San Lorenzo Quadrangles, Sierra and Grant Counties, New Mexico: U.S. Geological Survey Miscellaneous Field Studies, Map MF-900A, scale 1:48,000.
- , 1978a, Geologic map of the Gold Hill Quadrangle, Grant County, New Mexico: U.S. Geological Survey Miscellaneous Field Studies, Map MF-1035, scale 1:24,000.
- , 1978b, Geologic map of the Werney Hill quadrangle, Grant County, New Mexico: U.S. Geological Survey Miscellaneous Field Studies, Map MF-1038, scale 1:24,000.
- Kottlowski, F. E., Flower, R. H., Thompson, M. L., and Foster, R. W., 1956, Stratigraphic studies of the San Andres Mountains: *New Mexico Bureau of Mines and Mineral Resources Memoir*, v. 1, p. 1-132.
- Ludwig, K. R., 2001, Squid 1.02: Berkeley Geochronology Center Special Publication 2.
- , 2003, Isoplot/Ex 3.00: A geochronological toolkit for Microsoft Excel: Berkeley, Berkeley Geochronology Center Special Publication 4, 70 p.
- Maxwell, C. H., and Oakman, M. R., 1990, Geologic map of the Cuchillo quadrangle, Sierra County, New Mexico: U.S. Geological Survey Geologic Quadrangle Map GQ-1686, scale 1:24,000.
- Roths, P., 1991, Geology of Proterozoic outcrops in Dead Man and Little San Nicolas Canyons, southern San Andres Mountains, New Mexico, New Mexico Geological Society Guidebook, 42nd Field Conference, Sierra Blanca, Sacramento, Capitan Ranges, New Mexico Geological Society, p. 91-96.
- Seager, W. R., 1981, Geology of Organ Mountains and southern San Andres Mountains, New Mexico: *New Mexico Bureau of Mines and Mineral Resources Memoir*, v. 36, p. 1-97.
- Seager, W. R., Hawley, J. W., and Clemons, R. E., 1971, Geology of San Diego Mountain Area, Doña Ana County, New Mexico: *New Mexico Bureau of Mines and Mineral Resources Bulletin* 97, p. 1-38.
- Stacey, J. S., and Kramers, J.D., 1975, Approximation of terrestrial lead isotope evolution by a two-stage model: *Earth and Planetary Science Letters*, v. 26, p. 207-221.
- Stacey, J. S., and Kramers, J. D., 1975, Approximation of terrestrial lead isotope evolution by a two-stage model: *Earth and Planetary Science Letters*, v. 26, p. 207-221.

- Vollbrecht, K. M., 1997, Constraints on the timing and character of Proterozoic deformation and metamorphism in the San Andres Mountains of south-central New Mexico [MS thesis]: New Mexico Institute of Mining and Technology, 74 p.
- Williams, I. S., 1998, U-Pb by ion microprobe, *in* McKibben, M. A., Shanks, W. C., and Ridley, W. I., eds., Applications of microanalytical techniques to understanding mineralizing processes: Littleton, Colorado, Society of Economic Geologists, Reviews in Economic Geology p. 1-35.

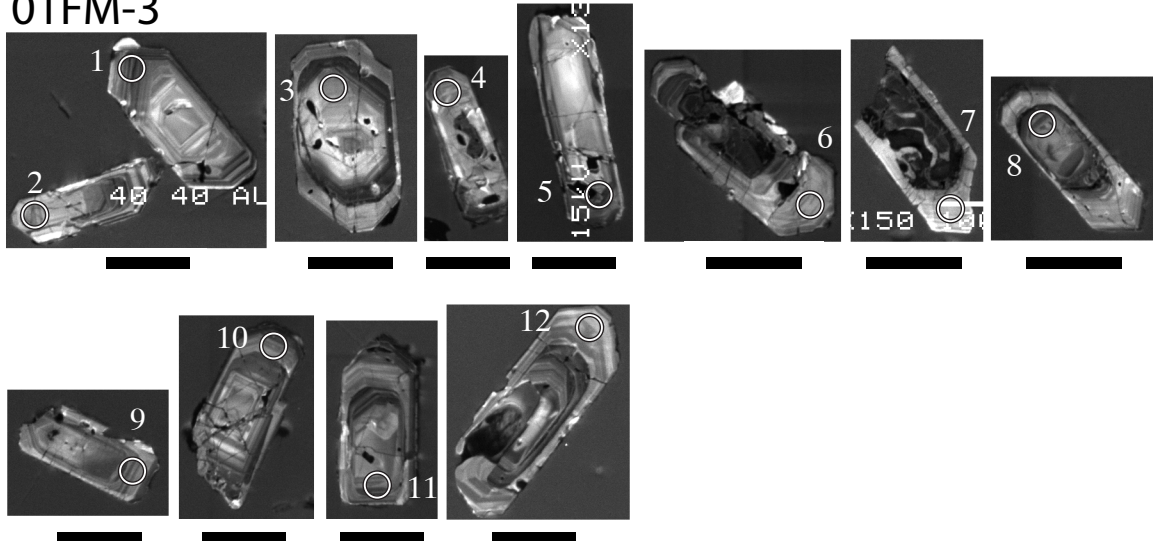
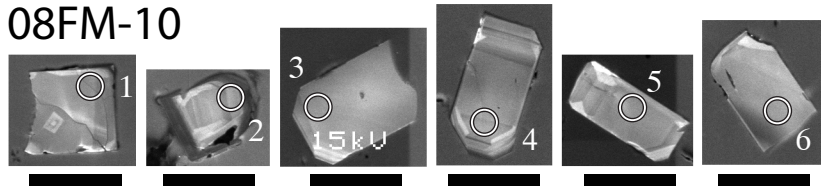
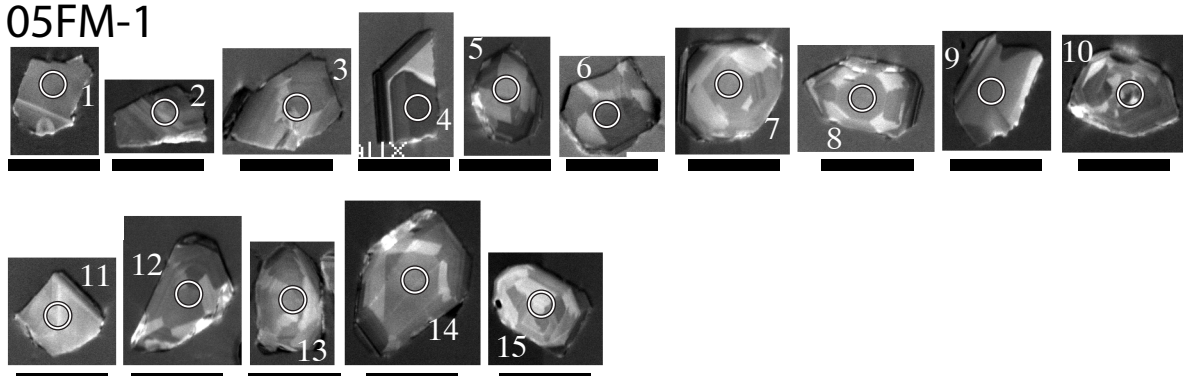
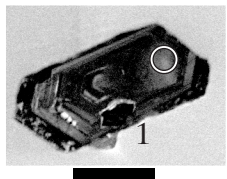
01FM-3**08FM-10****05FM-1****06SD-2**

Figure DR1: Cathodoluminescence images of igneous zircons from dated samples. Scale bars are 100 µm. Circles indicate analytical spot, with beam size of 30 µm. See Table 1 for locations and Table 2 for data corresponding to the numbered spots.

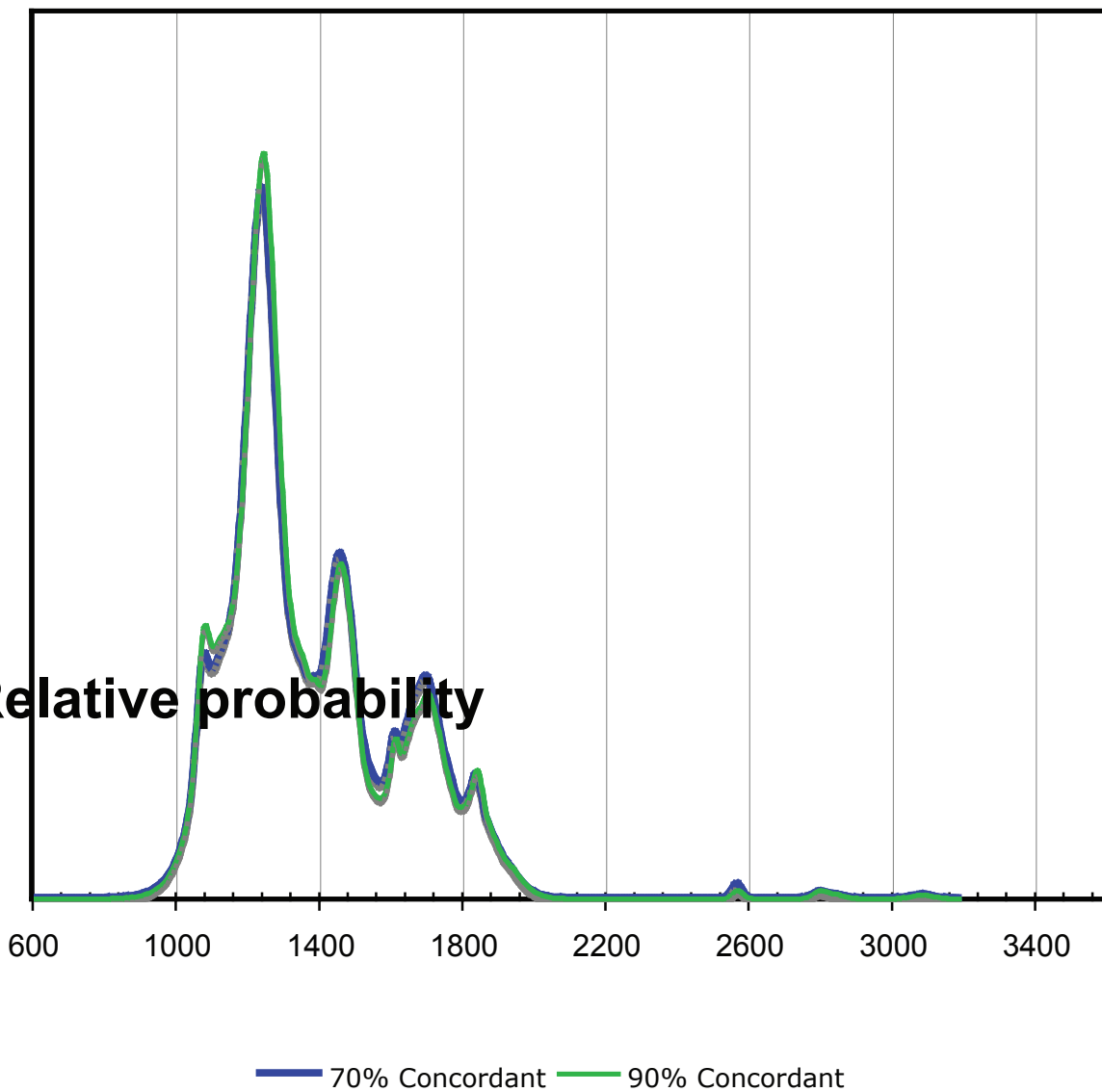


Figure DR2. Relative probability plots showing the difference between concordance filters of 70% and 90%. The two data sets are nearly identical because they are based on $^{207}\text{Pb}/^{206}\text{Pb}$ dates which are less sensitive to Pb-loss.

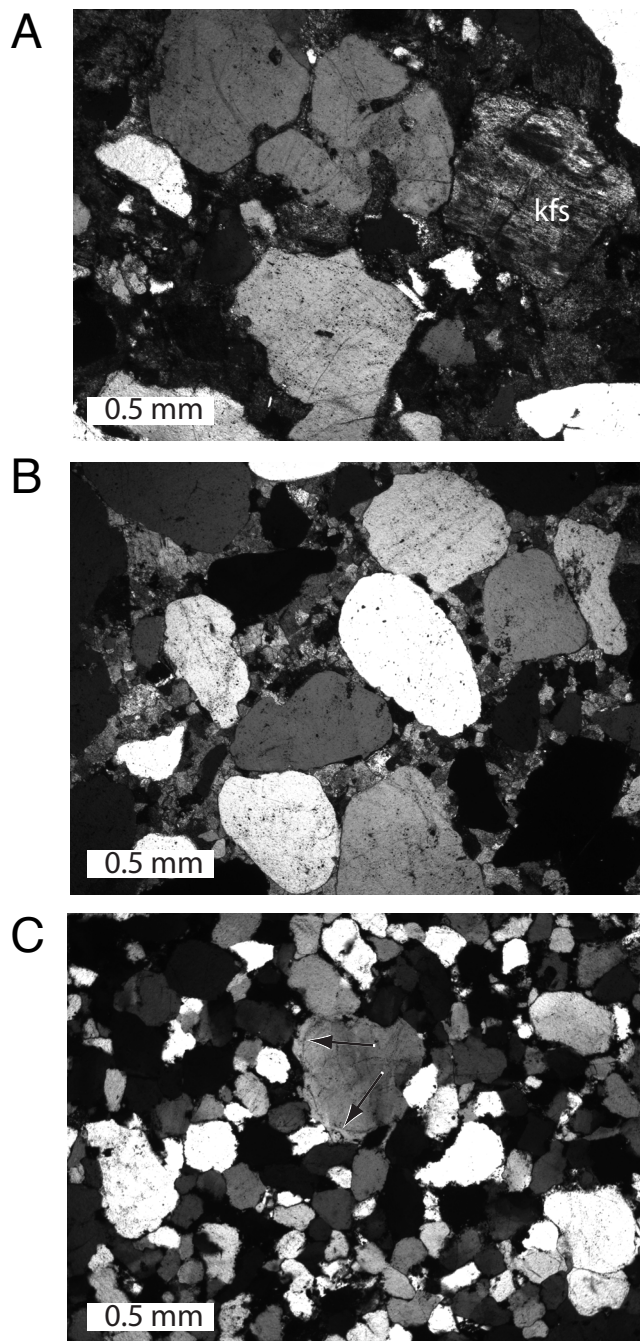


Figure DR3. Photomicrographs, all with crossed polars: (A) 08FM-9, lower Bliss at Florida Mountains, arkose, large K-feldspar grain noted, others are quartz; (B) 08FM-8b, upper Bliss at Florida Mountains, quartzarenite with rounded quartz and calcite cement; (C) 06SA-10, lower Bliss Sandstone at San Andres Mountains, quartzarenite with silica cement, arrows in large quartz grain pointing to edge of quartz overgrowth.

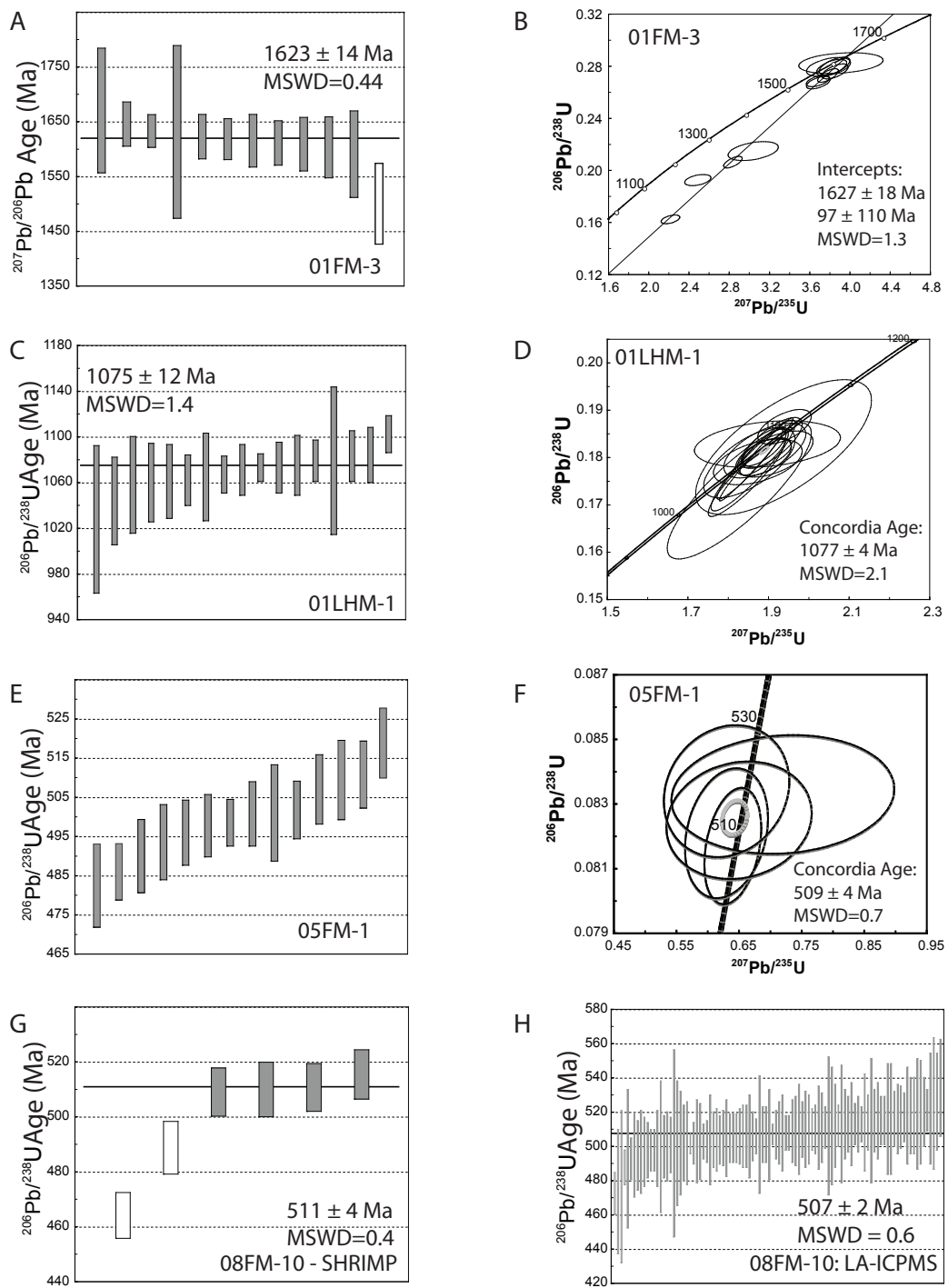


Figure DR4. Weighted mean plots and Concordia diagrams for intrusive rocks from the Florida Mountains. Error bars and ellipses are 1σ . On weighted mean plots, data bars with white fill were not used for age calculation. (A) weighted mean age of the Florida Mountains orthogneiss; (B) concordia diagram for Florida Mountains orthogneiss; (C) weighted mean age of the Little Hatchet Mountains granite; (D) concordia diagram for Little Hatchet Mountains granite; (E) weighted mean plot for the Florida Mountains granite; the pattern of descending ages without significant gaps is diagnostic of Pb loss, thus the oldest grains would provide the best estimate of the intrusive age; (F) concordia diagram of the Florida Mountains granite, using the oldest four analyses shown in (E); (G) weighted mean age of another sample of the Florida Mountains granite, using SHRIMP; (H) same sample of Florida Mountains granite as in (G), dated using LA-MC-ICPMS.

TABLE DR1. COMPLETE U/PB ZIRCON DATA COLLECTED BY SHRIMP

Spot	comm			$^{207}\text{Pb}/^{235}\text{U}$		$\% \text{ err}$		$^{206}\text{Pb}/^{238}\text{U}$		$\% \text{ err}$		$^{207}\text{Pb}^c/\text{corr.}^b$		^{206}Pb		$^{206}\text{Pb}/^{238}\text{U}$	age	$\pm 1\sigma$	$^{207}\text{Pb}/^{206}\text{Pb}$	age	$\pm 1\sigma$		
	$^{206}\text{Pb}^a$	U (ppm)	Th (ppm)	Th/U													(Ma)	(Ma)	(Ma)	(Ma)	% conc. ^d		
01FM-3: Florida Mountains orthogneiss																							
1	0.08	192	75	0.39	3.74	1.1	0.2697	0.8	0.695	0.1005	0.8					1548	12	1634	15	95			
2	0.08	163	53	0.32	2.80	1.3	0.2039	0.9	0.656	0.0997	1.0					1184	10	1619	19	73			
3	0.15	123	62	0.50	3.81	1.4	0.2728	0.9	0.617	0.1012	1.1					1564	13	1646	20	95			
4	0.60	141	55	0.39	2.46	2.1	0.1903	0.9	0.422	0.0937	1.9					1115	10	1501	37	74			
5	0.91	57	23	0.40	3.00	3.4	0.2122	1.4	0.414	0.1025	3.1					1227	16	1671	57	73			
6	0.64	69	29	0.43	3.86	4.4	0.2791	1.2	0.264	0.1004	4.2					1601	19	1632	79	98			
7	0.33	84	42	0.50	3.74	2.4	0.2762	1.1	0.451	0.0983	2.1					1588	16	1592	39	100			
8	0.25	159	64	0.40	2.19	1.7	0.1605	0.8	0.492	0.0989	1.5					941	8	1604	28	59			
9	0.18	217	101	0.47	3.64	1.3	0.2655	0.7	0.524	0.0994	1.1					1527	10	1612	20	95			
10	0.17	100	48	0.48	3.80	1.6	0.2769	1.0	0.608	0.0996	1.3					1590	15	1616	24	98			
11	0.23	188	75	0.40	3.64	1.3	0.2642	0.7	0.555	0.1000	1.1					1519	11	1624	20	94			
12	0.26	113	53	0.47	3.77	1.6	0.2757	0.9	0.575	0.0992	1.3					1584	14	1610	24	98			
06SD-2: San Diego Mountains granite																							
1	5.67	1297	449	0.35	1.65	2.4	0.1353	1.2	0.505	0.0886	2.1					797	9	1395	40	57			
08FM-10: Florida Mountains granite																							
1	0.26	140	101	0.72	0.61	3.3	0.0749	0.9	0.270	0.0589	3.2					464	4	563	70	83			
2	0.30	148	63	0.43	0.65	3.4	0.0822	0.9	0.259	0.0574	3.3					509	4	505	71.6	101			
3	0.45	160	112	0.70	0.60	3.9	0.0786	1.0	0.255	0.0554	3.8					489	5	428	84.6	114			
4	0.00	118	66	0.56	0.64	2.9	0.0822	1.0	0.332	0.0565	2.8					510	5	473	61.2	108			
5	0.28	146	103	0.71	0.65	3.8	0.0832	0.9	0.234	0.0569	3.7					515	4	487	82	106			
6	0.21	160	101	0.63	0.62	3.0	0.0822	0.9	0.289	0.0550	2.8					511	4	412	63.3	124			
05FM-1: Florida Mountains granite																							
1	0.38	161	102	0.63	0.67	2.3	0.0803	0.8	0.361	0.0607	2.2					496	4	627	47	79			
2	1.54	190	118	0.62	0.65	7.3	0.0825	0.9	0.122	0.0575	7.2					511	4	511	159	100			
3	0.20	220	142	0.64	0.64	2.7	0.0810	0.7	0.273	0.0573	2.6					502	4	501	57	100			
4	0.06	319	188	0.59	0.62	2.1	0.0803	0.6	0.282	0.0559	2.1					499	3	447	46	111			
5	0.14	117	83	0.70	0.63	4.3	0.0821	1.0	0.237	0.0560	4.2					509	5	451	93	113			
7	0.35	173	150	0.87	0.70	2.9	0.0813	0.8	0.289	0.0625	2.8					501	4	691	59	72			
8	0.46	201	169	0.84	0.63	2.6	0.0785	0.7	0.290	0.0586	2.5					486	4	553	54	88			
9	0.18	194	114	0.59	0.64	2.9	0.0817	0.9	0.309	0.0565	2.7					507	4	473	60	107			
10	0.15	160	111	0.70	0.63	2.5	0.0803	0.8	0.322	0.0570	2.4					498	4	492	52	101			
11	0.55	117	74	0.63	0.65	3.2	0.0792	1.0	0.301	0.0593	3.0					490	5	579	66	85			
12	0.19	222	172	0.77	0.63	6.5	0.0834	1.0	0.146	0.0547	6.5					518	4	401	145	129			
13	0.73	165	130	0.79	0.65	3.5	0.0781	1.1	0.322	0.0601	3.3					483	5	607	71	79			
14	0.47	221	187	0.85	0.64	3.0	0.0797	1.0	0.330	0.0586	2.8					494	5	553	62	89			
15	0.79	110	79	0.72	0.58	9.8	0.0803	1.3	0.136	0.0521	9.7					501	6	289	221	173			

a) Common Pb component (%) of total ^{206}Pb , determined using measured ^{204}Pb

b) Error Correlation coefficient

c) Ratio was corrected for common Pb using measured ^{204}Pb d) Concordance (%) = ($^{206}\text{Pb}-^{238}\text{U}$ age)/($^{206}\text{Pb}-^{207}\text{Pb}$ age) *100

Little Hatchet Mountains granite

LHM01-01	290	33202	1.9	13.132	0.9	1.84510	2.1	0.17573	1.9	0.91	1044	19	1062	14	1099	17	1099	17	95	30	11/21/11	2%
LHM01-02	160	94031	2.2	13.156	1.3	1.88742	1.5	0.18010	0.9	0.55	1067	8	1077	10	1095	26	1095	26	97	30	11/21/11	2%
LHM01-03	161	57150	2.0	13.165	1.1	1.89655	1.3	0.18109	0.7	0.52	1073	6	1080	8	1094	22	1094	22	98	30	11/21/11	2%
LHM01-05	139	50538	2.0	13.235	1.8	1.89080	2.2	0.18150	1.3	0.61	1075	13	1078	15	1083	35	1083	35	99	30	11/21/11	3%
LHM01-06	114	78675	2.0	13.221	1.1	1.90935	1.6	0.18309	1.2	0.75	1084	12	1084	11	1085	22	1085	22	100	30	11/21/11	2%
LHM01-08	262	151081	2.0	13.249	0.4	1.86938	2.0	0.17963	2.0	0.98	1065	19	1070	13	1081	9	1081	9	98	30	11/21/11	1%
LHM01-10	213	76397	2.7	13.308	0.9	1.88808	1.2	0.18224	0.9	0.71	1079	9	1077	8	1072	17	1072	17	101	30	11/21/11	2%
LHM01-11	126	77766	2.3	12.967	3.3	1.93744	4.6	0.18221	3.2	0.69	1079	32	1094	31	1124	67	1124	67	96	30	11/21/11	6%
LHM01-12	114	38827	1.8	13.317	1.9	1.85264	2.5	0.17894	1.7	0.66	1061	16	1064	17	1071	38	1071	38	99	30	11/21/11	4%
LHM01-13	115	97027	1.9	13.180	2.1	1.87355	2.4	0.17909	1.1	0.47	1062	11	1072	16	1092	42	1092	42	97	30	11/21/11	4%
LHM01-14	238	157914	2.0	13.204	0.9	1.86226	2.3	0.17834	2.2	0.92	1058	21	1068	15	1088	18	1088	18	97	30	11/21/11	2%
LHM01-15	176	84136	1.8	13.287	0.6	1.85372	1.8	0.17864	1.7	0.95	1060	17	1065	12	1075	12	1075	12	99	30	11/21/11	1%
LHM01-16	142	51740	2.0	13.049	2.2	1.82753	4.0	0.17296	3.4	0.84	1028	32	1055	26	1112	43	1112	43	93	30	11/21/11	4%
LHM01-17	188	134996	2.2	13.258	1.1	1.93969	1.4	0.18651	0.8	0.59	1102	8	1095	9	1080	23	1080	23	102	30	11/21/11	2%
LHM01-18	59	24984	1.7	13.287	3.7	1.89750	3.9	0.18285	1.1	0.28	1083	11	1080	26	1076	75	1076	75	101	30	11/21/11	7%
LHM01-19	192	130612	2.1	13.225	0.8	1.88895	1.3	0.18118	1.1	0.79	1073	11	1077	9	1085	16	1085	16	99	30	11/21/11	2%
LHM01-21	108	66874	2.0	13.002	1.6	1.91672	2.0	0.18075	1.1	0.56	1071	11	1087	13	1119	33	1119	33	96	30	11/21/11	3%